Ibn Al-Haitham Journal for Pure and Applied Sciences
Journal homepage: jih.uobaghdad.edu.iq
PISSN: 1609-4042, EISSN: 2521-3407
IHJPAS. 2024, 37(4)

Enhanced Electromagnetic Interference Shielding Effectiveness of Lightweight Polymethyl Methacrylate /Graphene/Silver Hybrid to Reduced Pollution and Healthcare

Badiaa I. Alawi[1] and Nadia A. Ali[2,*]
[1,2]Department of Physics, College of Science, University of Baghdad, Baghdad, Iraq.
*Corresponding Author

Received: 22 June 2023 Accepted: 20 August 2023 Published: 20 October 2024
doi.org/10.30526.37.4.3604

Abstract

The growth of using electronic devices has led to the development of a new pollution type that has been referred to as noise, radio frequency interference, or electromagnetic radiation (EM). The identification of lightweight PMMA/Gr/Ag nanocomposites has led to the discovery of a new hybrid polymer composite. Electrical conductivity, High Electromagnetic (EM) Shielding Effectiveness (SE) in a frequency range of 8.20-12.40GHz (x-band), dielectric characteristics, and differential thermal analysis were used to examine PMMA/Gr/Ag. Using the solvent casting process, a hybrid PMMA/Gr/Ag nanocomposite was created. The hybrid composite's electrical conductivity demonstrates that D.C conductivity is around 1.6×10-6 S/ cm as concentration is attained at 0.5% for Ag and 0.5% for Graphene, and that σac (ω) is frequency increases with increases in frequency. All PMMA/Gr/Ag nanocomposites exhibit decreasing dielectric properties (ε′, ε′′, tan δ) with increasing frequency. It was discovered that SE is highly dependent on Graphene and Ag, with the maximum SE attenuation recorded at 0.5wt% of Graphene and Ag being 11 dB at 12 GHz. Test of DTA shows that exothermic reactions with the dominating weight take place at (200–300)°C. PMMA matrix of PMMA/Gr/Ag nanocomposites displayed unique dispersion of the silver & graphene particles, according to FESEM results.

Keywords: Electromagnetic interference shielding, electrical conductivity, dielectric constant properties.

1. Introduction

The growth of the use of electronic devices has led to the development of a new pollution type that has been referred to as noise, radio frequency interference, or electromagnetic radiation

(EM). The identification of lightweight PMMA/Gr/Ag nanocomposites has led to the discovery of a new hybrid polymer composite. For the protection of electronics, especially those present in strategic systems like nuclear reactors, aircraft, control systems, transformers, and communication systems, among others, materials with EMI shielding properties are required. In comparison with traditional metal-based materials, the creation of EMI shielding materials depending on polymer composites has garnered more attention in academia and business. This is because they are more affordable, lightweight, and easy to manufacture [1]. Military radar stealth, electromagnetic shielding of cutting-edge electronic equipment, electromagnetic radiation protection, and other disciplines have all made use of the materials produced by the extensive use of electromagnetic waves. A significant amount of electromagnetic waves flow into the living environment because of the Internet and other electronic devices' rapid development, potentially impacting health and human life. To achieve wide bandwidth, high efficiency, and lightweight design, EMIS materials were created [2,3]. Because of their corrosion resistance, low density, affordable price, and superior processability, polymer matrix composites were extensively utilized in EMI shielding. Yet, most polymer matrices are inherently insulating, which significantly restricts their uses in electronic devices, medical equipment, new energy vehicles, flexible circuit boards, and other industries with demanding EMI shielding standards. As conductive fillers for polymer matrix composites, metal nanowires and particles, graphene, and carbon nanotubes have all been employed extensively [4,5].

Skin depth δ refers to the electromagnetic radiation's (especially microwave radiation) capacity for penetrating materials. This capability is important for telecommunication, radar-related applications, and EMI shielding [6]. Carbon-based conducting polymer nanocomposites have been discovered to be good EM shielding materials. Graphene was first functionalized through an acid treatment for attaching carboxylic functional groups to its surface for facilitating interaction with conducting polymer. polypyrene (PPy)/Graphene (GNS) and Polyaniline (PANI)/Graphene (GNS) nanocomposites [7]. When put to comparison with pure conducting polymers, it was discovered that the electrical conductivity of nanocomposites was significantly higher [8,9]. The use of dip-coated graphene on extremely porous PU sponges as low-density and compressible polymer/graphene composite (PGC) foams for the adjustable EMI shielding is still considered a difficult task. The resulting PU/graphene had good overall EMI shielding performance and an absorption-dominant mechanism, which may have been caused by the inside 3-D conductive graphene network's numerous EM wave reflections and scattering as well as conductive dissipation [10].

To test the EMI shielding, multi-layer graphene/polymer composite films with good mechanical flexibility have been fabricated into sandwich structures that are based on paraffin. The relation between electrical qualities and shielding effectiveness was demonstrated by the results, proving the importance of electrical properties in EMI shielding. To examine the fundamental mechanisms of reflection, absorption, and multiple reflections for polymeric graphene composite films, calculations depending on the electrical conductivity of composite films were made [11]. With the use of conductive graphene hybrid films, which are made up of a metallic network entirely encased between a quartz-glass substrate and monolayer graphene, EMI shielding capabilities have been fabricated and assessed. According to the findings, graphene sheet resistance has been dramatically reduced by integration with a metallic network, going from 813.27Ω/sq to 5.53Ω/sq with a 91% optical transmittance [12].

Because of their broad bandwidth properties in comparison with traditional metal-based materials, corrosion resistance, low cost, adaptability, lightweight, and simple processability, graphene-enhanced polymer composite materials have lately been presented as metal-based EMI shielding

material replacement. Maxwell's equations could be solved analytically or numerically to obtain the SE from bulk material parameters, such as permeability, permittivity, and conductivity. However, graphene-based polymer composites are heterogeneous. Using the predetermined characteristics of polymer matrix and carbon-based filler, the model is intended for predicting the electromagnetic properties related to nanocomposite [13]. The research aims to use metal-based polymer in EMI shielding materials mostly focused on super high frequency (SHF) specifically in X-band.

2. Methods and Material

2.1. Experimental Procedure

Through using the solvent casting technique, PMMA/Gr/Ag hybrid nanocomposite films have been fabricated. To create a stable suspension, newly synthesized (Ag supplied by Sigma-Aldrich was (99.8 % purity, specific surface area of 25 m^2/g) with a particle size of 85nm. and graphene whose average diameter of 69.22 nm is shown in **Figure 1.** measured by (SPM) have been dispersed ultrasonically in chloroform for two hours. The solution was next combined with a 3g PMMA solved in chloroform to create a PMMA/Gr/Ag mixture that had 0.1, 0.2, 0.3, 0.4, and 0.5% (Graphene) and a constant (0.5%) Ag content. To get a uniform dispersion of Graphene, and Ag in PMMA, the mixture was once again ultrasonically processed for two hours. This solution was poured into a Petri dish (diameter 4cm) that had been sprayed with Teflon to create a thin polymer coating. Nanocomposite films were dried at 25ºC for 24h following the solvent's evaporation, after which they were taken out of dishes and sliced for characterization and physical study. The final film was roughly 0.25 mm thick.

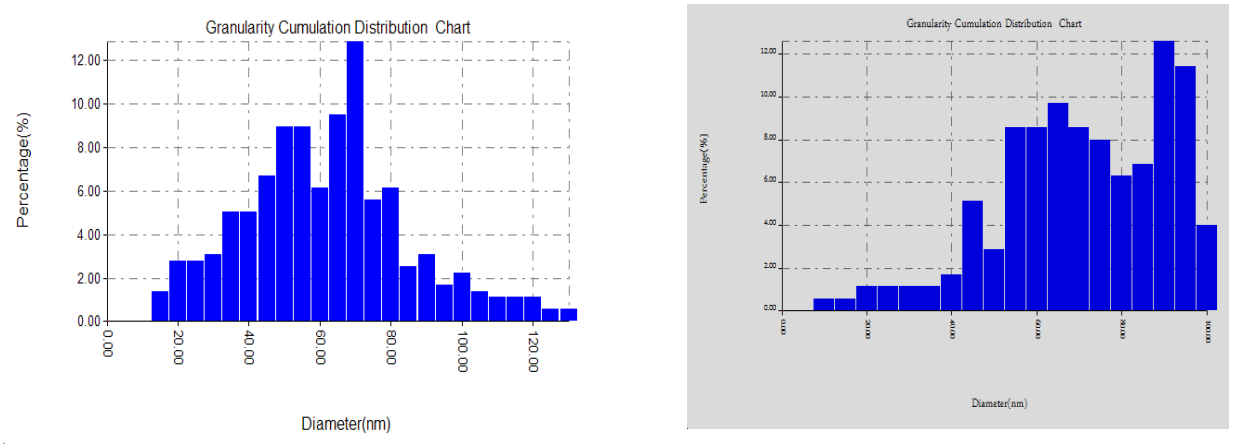

Figure1. AFM analysis images of silver, and graphene nanoparticles used in the work.

2.2. Characterization of Nanocomposites

2.2.1 Fourier Transform Infrared (FT-IR) Analysis:

The infrared spectra were recorded with the help of Shimadzu type FTIR -7600 in the range 400 to 4000 cm^{-1}.

2.2.2 Field Emission Scanning Electron Microscopy (FESEM)

With an unlimited depth of field, FESM offers elemental and topographical information at magnifications ranging from 10x to 300,000x (model S-4800, Hitachi, Japan).

2.2.3 Electrical properties

With the use of the (ρ) of the films, the electrical Resistance was measured between (303-393K) with the use of the next equation. [14]. D.C. measurements have been done using a sensitive digital electrometer type Kethley (616) to measure the current, as well as the D.C. power supply (2 Volt) A.C. measurements have been achieved using HP-RLC unit model 4274A and 4275 multi-frequency LRC meter, in the range of (10kHz–100 MHz), with amplitude of 0.08 volt and zero bias.

$$\rho = \frac{R.A}{L} \quad (1)$$

Where: R represents the sample Resistance, A represents the film's cross-section area and L represents the samples' thickness. The films' conductivity was specified from the relation:

$$\sigma dc = \frac{1}{\rho} \quad (2)$$

The σ is determined by the Arrhenius equation and varies exponentially with (T), which is derived by Equation 3.

$$\sigma dc = \sigma_o \, e^{-Ea/KT} \quad (3)$$

The σ has been calculated from the next Equation 4:

$$\sigma t(\omega) = \frac{d}{RA} \quad (4)$$

where (d) represents the sample's thickness and (A) represents the cross-section area. A.C conductivity σac (ω) has been computed with the use of relation:

$$\sigma t(\omega) = \sigma ac(\omega) + \sigma dc \quad (5)$$

$$\sigma ac(\omega) = \sigma t - \sigma d.c = A\omega^s \quad (6)$$

In which σdc represents D.C. conductivity. (A) represents a constant independent of the temperature, (ω =2*π*f), and (s) represents the frequency exponent.

The dielectric permittivity of a material (ε) can be described as a complex quantity with a real part (εr) and imaginary part (εi) and it is given by Equation 7 [15].

$$\varepsilon = \varepsilon r + \varepsilon i \quad (7)$$

The real and imaginary part values of the dielectric permittivity εr and εi can be estimated from the capacitance value that is measured in the parallel mode (Cp) and loss tangent (tan δ). Cp and tan δ values are measured for the temperature of the room and range of frequency of 10 kHz–100 M Hz. The εr and εi values are estimated based on Equations 8 and 9:

$$\varepsilon' = Cd/A\varepsilon o \quad (8)$$

$\varepsilon'' = \varepsilon' \tan(\delta)$ where $\delta = 90 - \varphi$ (9)

$\tan \delta = \varepsilon''/\varepsilon'$ (10)

where εo represents free space permittivity and d and A represent the sample's thickness and cross-section area, respectively.

2.2.4 Electromagnetic Interference Shielding Effectiveness

With the use of the waveguide method (closed system) the samples' electromagnetic characteristics are measured at an x-band frequency in 1.3 cm preparation samples and cut (2.29×1.02 cm^2) **Figure 2**. 8.2–12.4 GHz. EM parameters were measured on a vector network analyzer (E5062A/EM2107A, Agilent Technologies, Santa Clara, CA, USA). Incident and transmission powers are used to calculate the shielding effectiveness. Using a network analyzer and the coaxial line approach as described in [16]. Using the following Eq (11), SE was determined and expressed in decibels (dB): EMI SE (SE_{total}) is represented by the summation of contributions from reflection loss (SE_R), absorption loss (SE_A), and multiple reflections (SE_M) [17].

$SE_{total} = SE_A + SE_R + SE_M$.) (11)

2.2.5 Differential Thermal Analysis Device (DTA)

It describes how to measure Tg and Tm, With the use of a TG-209F (STA PT-1000 linseis, Germany) with a heating rate of 10°C/min under nitrogen flowing at a rate of 50ml/min, samples of about 10–19mg were provided at Td of 25–400°C.

3. Results and Discussion

Figure 3. displays the PMMA film's FTIR spectrum and details the functional groups present in the PMMA preparation film. Two main areas stand out: the diagnostic region on the left, which is located between 1500 and 4000 cm^{-1}, and the fingerprint region, which is located between 400 and 1500 cm^{-1}.

The left region is close to 4000 cm-1 because it contains high energy bonds. The O-H (stretching vibration) is represented by the peak at 3414cm^{-1}, while C=O (stretching vibration) from PMMA

is characterized by the absorption band at 1732cm^{-1}. The C-O stretching vibration in PMMA is shown by the absorption band at 1147 cm^{-1}. The absorption band at 1242 cm^{-1} indicates C-C from PMMA, while the absorption band at 2951 cm^{-1} corresponds to C-H stretching in that region. Due to the ester carbonyl group's (C = O) stretching vibration, a sharp, intense peak at 1736 cm^{-1} has been seen. The stretching vibration of the C-O (ester bond) could be used to explain the broad peak spanning from 1260 to 1000cm-1. The bending of C-H is what causes the broadband from 950-481cm-1. One explanation for the peak at 2935 cm1 is C-H stretching, which is consistent with agree with [10].

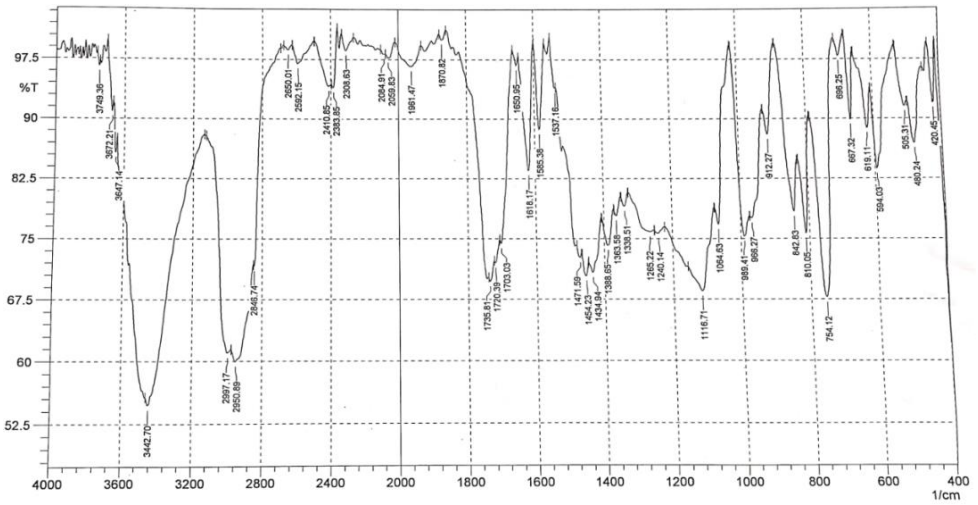

Figure 3. FTIR of pure PMMA

In the PMMA/Gr /Ag nano nanocomposites in **Figure 4** the peaks at 610 C–H cm^{-1}, 842 cm^{-1} of C–C stretching, 1086cm^{-1} C–O stretching, 1242 cm^{-1} C–OH stretching, 1372 cm^{-1} plane OH bending mode of hydroxyl groups, 1732 cm^{-1} C=O stretching,2901 cm^{-1} and 3395 cm^{-1} O–H stretching vibration, peak for graphene between 3000cm -1 and 3500cm -1 (O-H) as a result of the absorbed moisture that returns to (C-OH) carboxylic acid, with (C=O) 1733cm^{-1} (carbonyl/carboxy), (C=C) 1631cm $^{-1}$ (aromatics), (C-O) 1358cm $^{-1}$ (carboxy), (C-O) 1047cm^{-1} (alkoxy). The peak was observed at 1668 cm^{-1} due to the C=C stretching. The maximum peak has been at 3420 cm^{-1} (stretching and bending vibrations of the –OH group), and 1245 cm^{-1} has been assigned to C–OH, and the peak centered at 1615cm^{-1} has been assigned to the C=C bonds related to skeletal vibrations of the unoxidized graphitic domains. C=O bonds in the fragments of carboxylic acid and carbonyl were assigned to the peak at 1730 cm^{-1}. At 1420 cm^{-1}, the G-Ag NPs showed a new stripe due to G-Ag's diminished C-N stretching vibration. Additionally, the C-OH bond was assigned to the absorbance peak at approximately 1270 cm−1, and the skeletal vibration of graphene sheets was given credit for the absorbance stripe at 1515 cm^{-1}.

Figure 4. shows the FT-IR spectra of PMMA/GMA/Ag nanocomposites, in which the C=C characteristic peak at 1638 cm^{-1} essentially disappeared to signify the nearly total copolymerization of the MMA/GMA monomers. In the spectra of PMMA/ GMA/Ag nanocomposites, the C=O characteristic peak at 1729 cm^{-1} has also been moved to a higher value

at 1740 cm^{-1}. Ag-NPs and the polymer matrix may have interacted, as evidenced by the relative improvement in the strength of the CH absorption peak at 2996.84 cm^{-1} and 2952.48 cm^{-1}.

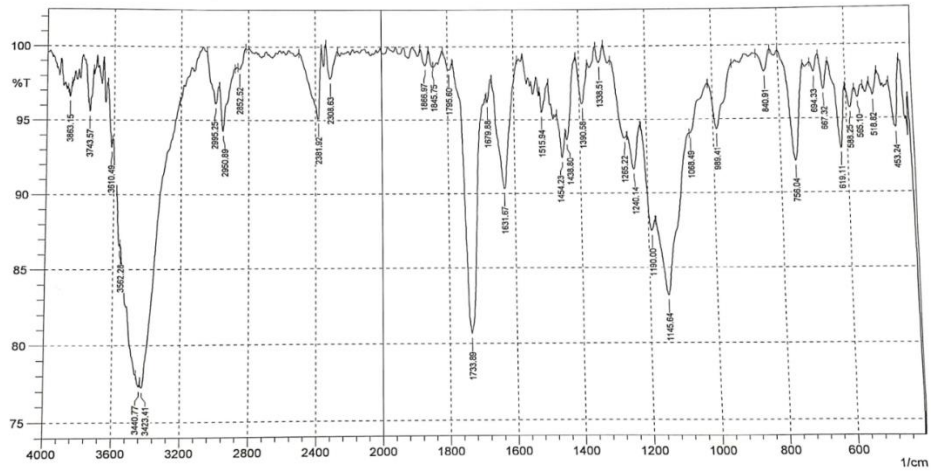

Figure 4. FTIR of PMMA/Gr /Ag hybrid composites

Figure 5. depicts the connection between Lnσdc and the inverse absolute temperature of nanocomposites. According to the findings, the electrical conductivity increased with the increase of the concentrations of Ag and Gr, going from 3.21×10-9 S/cm to 1.6x10-6 S/cm.

Gr concentration rises from 0.1% to 0.5% for PMMA/Gr/Ag nanocomposites. **Figure 3.** illustrates the impact of the hybrid fillers in the samples. Pure PMMA exhibits values of 3.21×10-9 S/cm, while composites with low loadings of Gr/Ag (up to 0.1/0.5 wt%) likewise have a value of 7.52×10-9 S/cm. An abrupt increase of σ up to ~3 orders of magnitude is seen above this Gr concentration and up to (0.5/0.5 wt%), indicating the onset of electrical percolation. By raising the Gr loading even more, σ keeps rising until it reaches a maximum value (σmax) of 1.6×10-6 S/cm up at (0.5/0.5 wt%0 of Gr loading when it plateaus.

To improve the conductivity behavior of the composites, Ag-NP is added. This suggests that the presence of nanosilver has an impact on the overall electrical characteristics of the polymer composite with a polymer threshold of approximately 0.5% because Ag was majorly utilized as a conductor wire in circuits that require high conductivity and short tunneling distance and poor percolation resistivity decreases percolation resistance and results in more favorable conditions for the transfer of electrons between neighboring fillers, which improves conductivity in the composites. The equation (12) could be used to investigate the electrical percolation behavior.

$$\sigma = [\ (\phi - \phi_c) / (1 - \phi_{c)}\ ]^t \qquad (12)$$

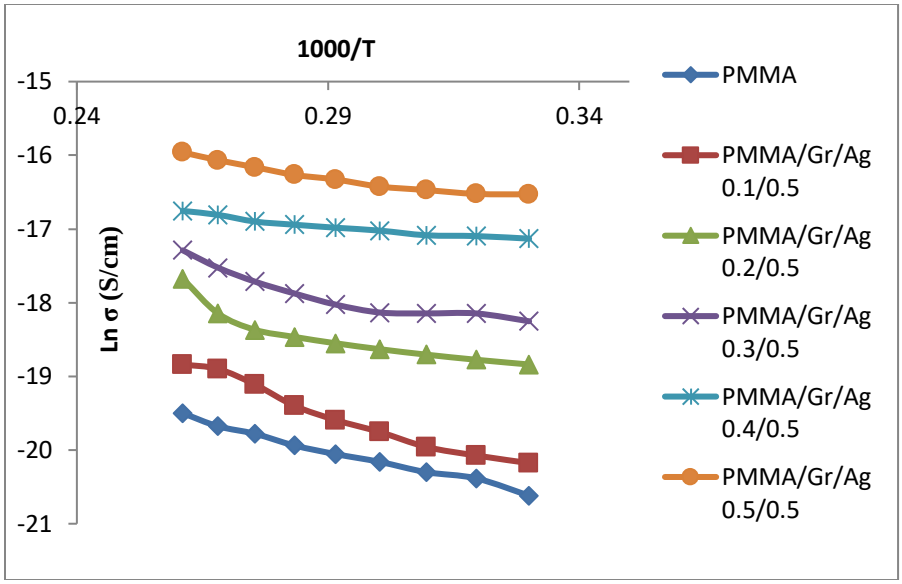

Figure 5. Electrical conductivity& 1000/T of PMMA/Gr/Ag hybrid composites

For $\phi > \phi c$, in which ϕ represents the filler's volume fraction, ϕc represents the population threshold in volume fraction and t represents the universal critical exponent. A 2D percolating structure is expected to have a value of about 1.3 (**Table 1**). The parameter t is frequently utilized for characterizing the kind of percolation of the system [18].

Table 1. Electrical conductivity of PMMA/Gr /Ag hybrid composites

sample	electrical conductivity S/cm	Ea (eV)
PMMA	3.21×10^{-9}	2.36
PMMA/Gr/Ag 0.1/0.5	7.52×10^{-9}	2.2
PMMA/Gr/Ag 0.2/0.5	2.63×10^{-8}	2.05
PMMA/Gr/Ag 0.3/0.5	4.21×10^{-8}	1.98
PMMA/Gr/Ag 0.4/0.5	6.19×10^{-7}	1.90
PMMA/Gr/Ag 0.5/0.5	1.6×10^{-6}	1.66

When the activation energy of PMMA/Gr nanocomposite was characterized using Equation 3, results revealed high activation energy values that range between 2.36 and 1.66eV. The existence value of the activation energy in polymer nets is summarized in Table 2. Because of the effect of space charge, adding small amounts of graphene nanosheets (Gr) causes a decrease in the values of the activation energy of the samples. In the forbidden energy gap, it also generates local energy levels that interact to confine charge carriers which travel by hopping between levels that meaning Electrons are not present in a forbidden gap because the energy levels within the gap do not align with the energy levels of the electrons. In a semiconductor, the forbidden gap is a range of energy

levels that lies between the valence band (the band of energy levels occupied by electrons in the outermost energy level of the atom) and the conduction band (the band of energy levels that are unoccupied by electrons). Because the energy levels within the forbidden gap do not align with the energy levels of the electrons, the electrons cannot occupy that region of energy. As a result of increasing the local centers of the nanocomposite, raising the loading ratio of Gr lowers activation energy [19]. Figure 6 shows the A.C of PMMA at frequencies between 10KHz and 10MHz at 23C along with different concentrations of Gr & Ag included.

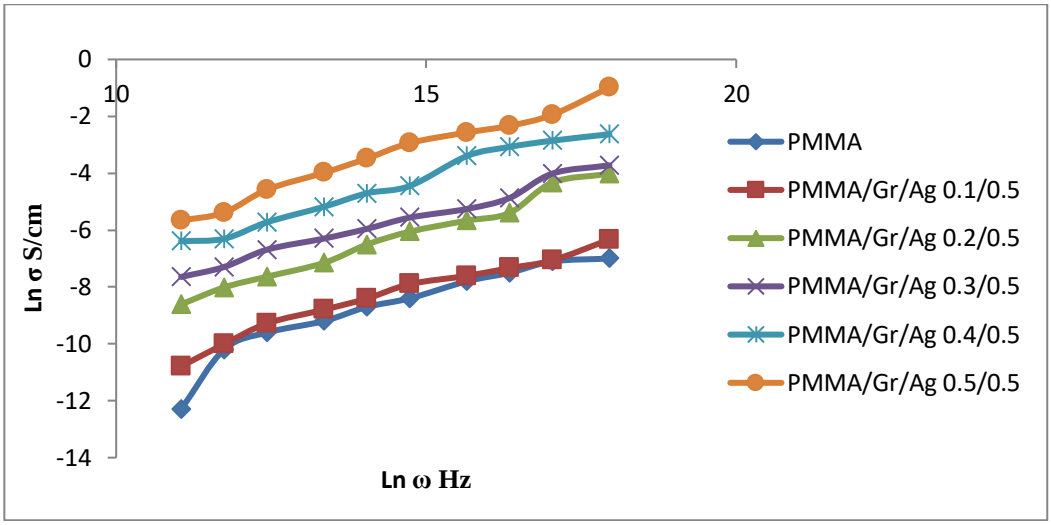

Figure 6. AC conductivity of PMMA with various contents of Gr/Ag/PMMA

The connectivity and electron transport mechanism of Gr, Ag network in the polymeric matrix is revealed by the hybrid composites AC. It has been found that all samples conductivities rise with increasing frequency, but PMMA's conductivity is lower than that of its Gr, Ag. This could be explained by dipoles' propensity to align themselves with the applied field in polymeric samples (Liu, W, et al. 2017). By deducting the A.C conductivity from the total conductivity measured using Equation (6), the A.C conductivity is obtained.

Figure 6. illustrates the fluctuation of σac (ω) as a function of the frequency of PMMA/Gr/Ag hybrid composites at various ratios. (4). The dominance of A.C. conductivity, in which the polarization is slightly altered, is the cause of σac (ω) which is clearly frequency dependent for both pure PMMA and for (0.5/0.5wt%) hybrid composites, i.e., the conductivity is pure A.C, and this is due to the electronic polarization. The plot of ln(σtot(ω)) & ln(ω) for PMMA/Gr/Ag hybrid composites at various ratios provided the (s). For all samples of composites, values of s are quite lawful, as shown in Table 2. The exponential factor (s) is smaller than one shows that conductivity occurs during hopping that reflects the percentage of reactants who have approached and crossed the activation energy hill in the number of tries. The average values of (s) seem to agree with charge carriers (protons) hopping across polymer chains [14]. All of the PMMA/Gr/Ag nanocomposites have had their dielectric characteristics examined.

Table 2. The exponential factor of PMMA/MWCNT/Ag hybrid composites.

Samples	S
PMMA	0.94
PMMA/Gr/Ag 0.1/0.5	0.66
PMMA/Gr/Ag 0.2/0.5	0.65
PMMA/Gr/Ag 0.3/0.5	0.58
PMMA/Gr/Ag 0.4/05	0.56
PMMA/Gr/Ag 0.5/0.5	0.50

Figures 7. and **8.** show the dielectric loss and dielectric constant vary with frequency for all composites; at higher frequencies, the loss becomes nearly constant at lower concentrations of graphene, while at greater concentrations of silver that means the dielectric behavior of all fabricated samples was dependence on the graphene content within the PMMA matrix was analyzed, the influence of the graphene and silver concentration on the dielectric properties of the composite material at lower frequency, the behavior being similar at other frequencies up to 1 MHz. seen, the dielectric constant increases almost linear with graphene concentration, becoming double at a concentration of 0.5%. In contrast, the respective dielectric losses present a significant reduction, becoming four times smaller at the concentration of 0.5%. Regarding the variation of the dielectric constant with frequency, this is shown in **Figure 9.** for a sample containing 0.3% graphene. As can be observed, increasing frequency results in a quite important decrease in the dielectric constant value.

The frequency decreases and ε' and ε" drop with frequency. Because there are two types of dielectric losses this suggests that dipoles are arranged along field directions at low frequencies to increase overall polarization meaning metallic nanofillers in appropriate amounts can improve the dielectric property of polymer composites. When conductive metal nanofillers are added to a polymer matrix, space charges (electrons and holes) accumulate at the metal-polymer interfaces to trigger IFP occur. Although the permittivity of metal-polymer composites is generally high, many unsolved issues still exist. Conduction loss is caused by the movement of charges that experience resistance or friction, which leads to energy dissipation in the form of heat. In theory, as the number of conductive fillers in a polymer increases, the distance between the filler particles becomes smaller. Conduction loss is caused by the real charge flowing into the dielectric, and dielectric loss is caused by molecules or atoms rotating in an alternating current field [21]. Figure 9 illustrates how the value of loss tangent rises with frequency, reaches a maximum at a particular frequency, and after that falls at higher frequencies. The absence of dielectric materials to follow the applied electric field causes a loss tangent to arise, which causes warmth creation.

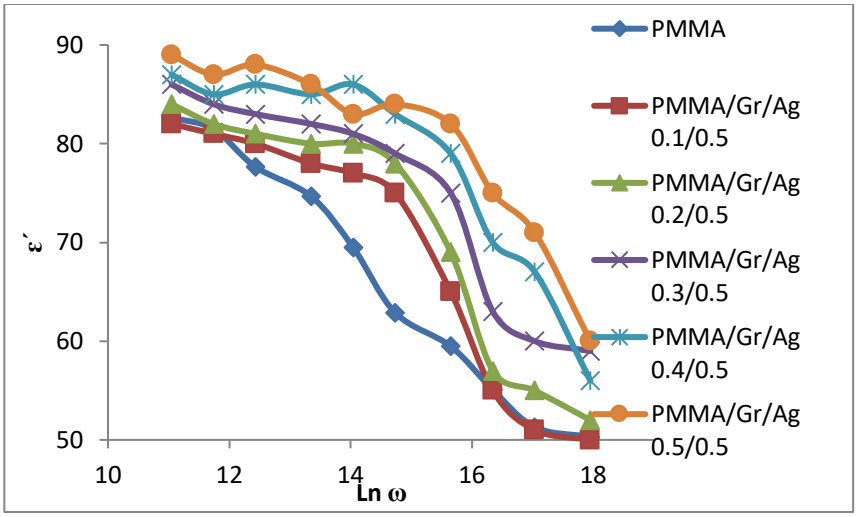

Figure 7. Dielectric constant ε´, versus Lnω for PMMA/Gr/Ag hybrid composites at the temperature of 323 K.

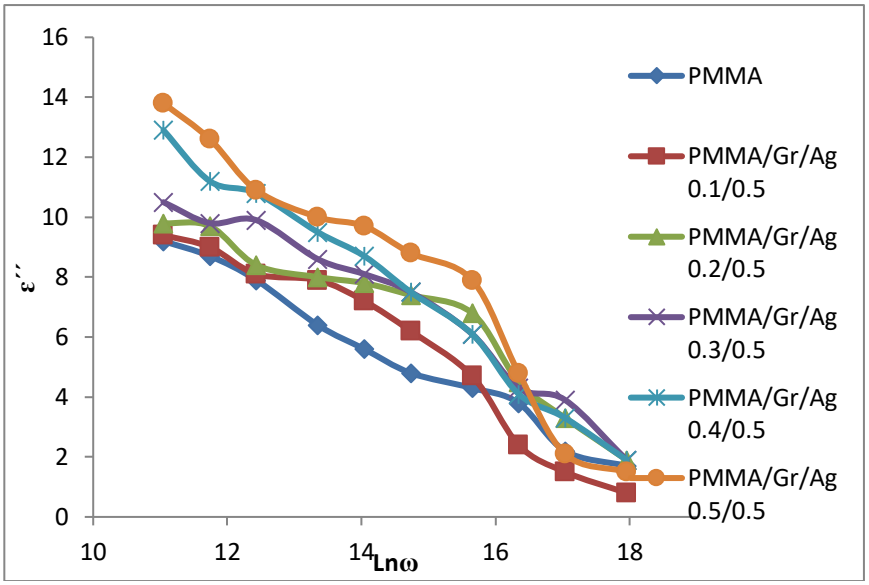

Figure 8. Dielectric Loss ε´´, versus Lnω for PMMA/Gr/Ag hybrid composites at the temperature of 323 K.

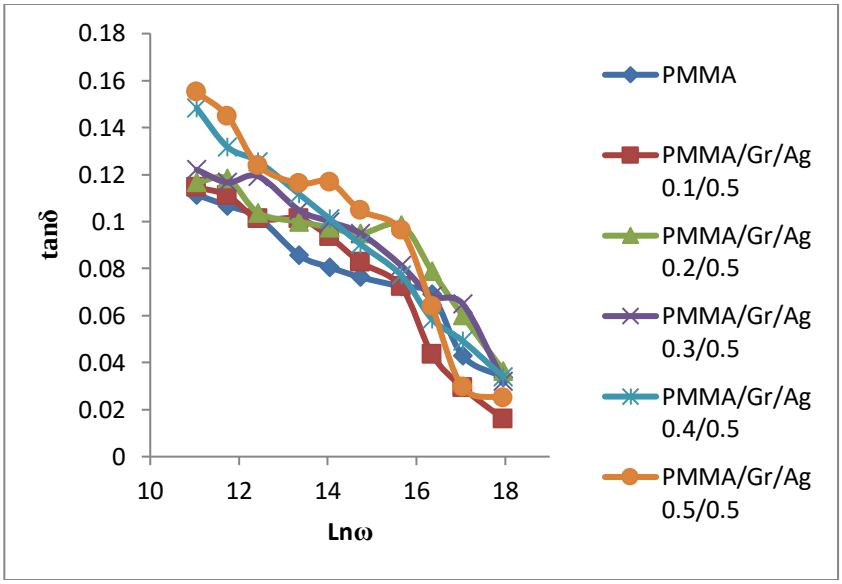

Figure 9. Loss tangent tan δ, versus Lnω for PMMA/Gr /Ag hybrid composites at the temperature of 323 K.

Figure 10. depicts the results of the EMI shielding effectiveness (EMI-SE) measurements performed in the X band frequency range (8–12.4 GHz). The efficacy of a material's shielding against EMI is determined by how well it can attenuate electromagnetic waves. In comparison to PMMA (at ω=12.4 GHz), graphene and Ag demonstrated improved EMI shielding efficacy. More scattering results from increased interfacial polarization and effective anisotropy energy of the sheets as a result of the Gr-containing polymer matrix. Comparing the materials to traditional materials, the materials also exhibit a high shielding effectiveness. The penetrating EM waves will be attenuated by the synergism between Gr, Ag and PMMA matrix via dipolar polarization loss, interfacial polarization loss and conduction loss. Furthermore, the enormous number of solid/air interfaces created by the microcellular structure can effectively extend the path of propagating EM waves via internal multiple reflections and scattering, further attenuating the propagating EM waves.

With increased Gr, Ag concentration, the nanocomposites' EM shielding performance rises. The volume resistivity of composites reduces and their efficacy and shielding rise as Gr is increased from 0.1% to 0.5%. As Gr amounts rise, the number of percolating networks also rises. The conductive networks created because of Gr's dispersion exhibit conductive mesh-like behavior. The size of conductive mesh shrinks as Gr loading rises, serving as a barrier to incident electromagnetic radiation and increasing EMI SE. This is because a composite's electrical conductivity tends to rise with increasing Gr content, and under the influence of EMI, an induction current generated on the interface or in the interior of the sample produces a reversal electromagnetic field, which increases the surface reflection attenuation of EMI and raises the composite's EMI shielding effectiveness. [22]. Ag is one of the possible materials for shielding applications due to its extremely high electrical conductivity. For the successful creation of composite materials for EMI shielding applications, Ag-based nanostructures are utilized. Since a high aspect ratio of a nanowire is beneficial for constructing a highly percolated network structure

and achieving high conductivity, Ag nanowire polymer nanocomposites were researched extensively as shielding materials [23,24]. To create a high-reflection type EMI shielding polymer hybrid, other requirements must be met in addition to the filler's high conductivity. Having a percolated threshold network with less filler content is the main need.

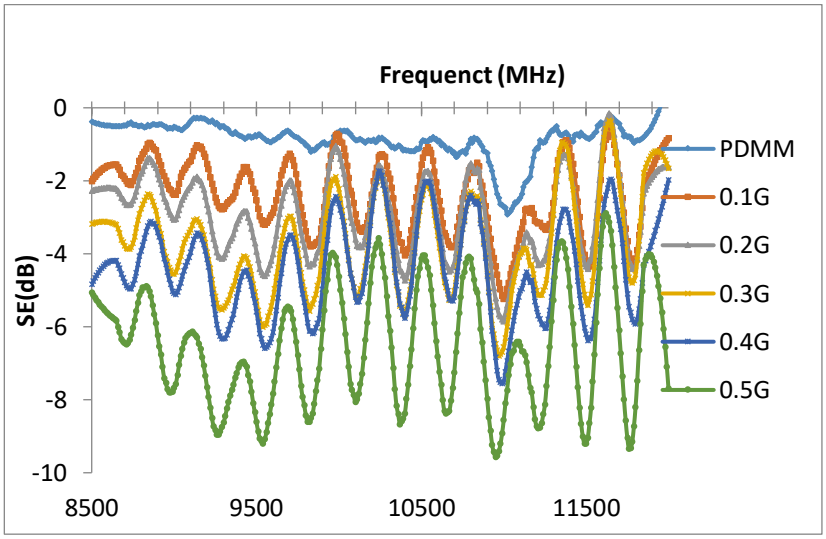

Figure 10. Electromagnetic interference (EMI) shielding of PMMA/Graphene/Ag hybrid composites

The melting peak shifts to a lower temperature and appears at (153.84 ºC), (138.57 ºC), and (119.63 ºC), respectively, in **Figure 11.** DTA and TGA curves of pure PMMA and PMMA/Gr/Ag. These curves reveal one mass endothermic peak that reflected the melting point of the raw materials (PMMA, Ag, and Gr). The curve demonstrates a strong endothermic process beginning at 128.62 °C -165.32 °C and 108.92 ºC-137.88 ºC, respectively. The level of adsorption is typically higher the higher the molar mass of PMMA. This is expected since only a portion of the polymer chain was adsorbed; the remaining portion is more likely to adsorb the Graphene surface through CH interactions. Given the existence of amorphous carbon and other impurities, graphene has been demonstrated to preserve its structure in an inert atmosphere at temperatures beyond 800 °C [25]. However, there has been very little mass loss. Adding additional graphene causes PMMA to adsorb since more MWCNT surface area is accessible, allowing for more polymer to do so.

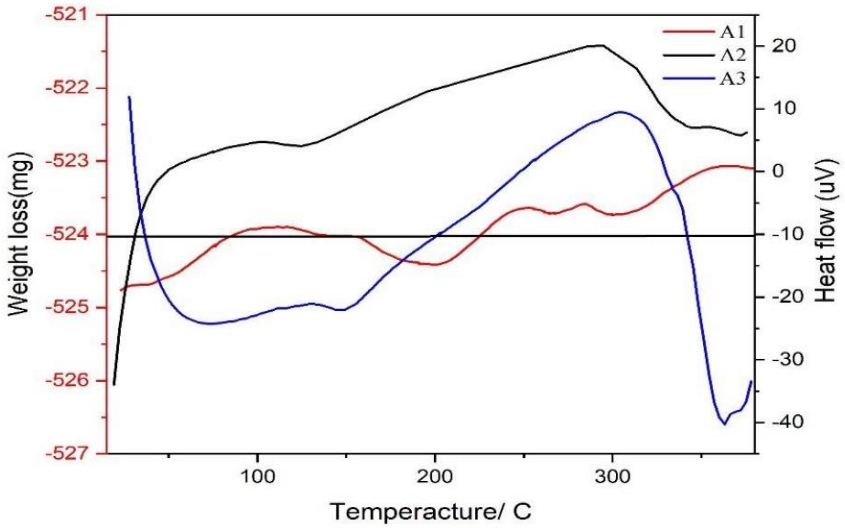

Figure 11. Differential Thermal Analysis of PMMA(A1), PMMA/Gr/Ag /Gr (0.1/0.5%) (A2), PMMA/Gr/Ag at (0.5/0.5%) (A3) hybrid composites

PMMA/Gr/Ag at (0.1/0.5%) TGA/DTA schematic trace. The 0.5/0.5% sample exhibits weight loss due to the carbon layer's thermal decomposition, which begins around 279–309 °C and 278–305 °C. The DTA diagram's exothermic peak, which is centered at 288 °C and 290 °C, respectively, denotes the exothermic curves caused by the crystalline phase of composites and thermal decomposition. The curve of TGA-DTA plots is depicted in Figure 9 to demonstrate how they are frequently used to analyze composition of water, combustion carbon, volatile compounds, and impurities in graphene and materials that are related to it. We concentrated on thermal parameters (i.e. temperature of the maximal mass change rate, T_{max}) in this investigation. The maximum peak position in the negative region of DTA curve could be utilized for the purpose of computing T_{max}, which refers to the final mass loss step that is related to the combustion of the carbon.

Since a 5% sample weight loss, the starting temperature of thermal degradation (Tonset) was taken into consideration. The results of TAG indicated that adding graphene improved the thermal stability of the blends. This enhancement could be attributed to graphene's higher thermal stability when compared to polymer phases, its high thermal conductivity as nanoplatelets, and its interaction with polymer phases, which results in more uniform development and higher thermal conductivity matrix and that t h e interface adhesion between nanosheets, and matrix was dramatically improved. Additionally, for the Gr-filled samples, the inflection points of diagrams (the maximum points of the derivative of curves) showing the maximum weight loss of samples have manifested at higher temperatures [26]. It is well known that the good dispersion of nanoparticles and the strong interfacial interaction with the polymer are two important factors in improving the physicochemical properties of nanocomposites. The presence of graphene filler facilitates heat transfer in the sample volume, thereby reducing the thermal decomposition temperature. High thermal conductivity begins to play a significant role at high graphite filler

concentrations. The process is more efficient the more homogeneous the composite structure is. The homogeneity of the structure is influenced by the grain size of the filler [10].

FESEM analysis of PMMA/Gr/Ag at (0.1%/0.5%) and (0.5%/0.5%) nanocomposites is exhibited in **Figure 12.** reveals a uniform integration as well as distribution of the filler particles by PMMA matrix with a homogenous deposition of prepared PMMA/Gr/Ag nanocomposites with concentrations of Ag-NPs (0.5%wt) in **Figure 12**. The films show a uniform density of grain distribution at surface morphology. Also, surface morphology that is related to the (PMMA/Gr/Ag) hybrid nanocomposite films demonstrate numerous aggregations or chucks of (Gr, Ag) nanocomposites that are distributed randomly on films' top surface.

The results showed that (Gr, Ag) particles tend to form aggregation and are well dispersed at films that are randomly distributed in PMMA composite films, and it was determined that small agglomerations is formed in these films. According to SEM images, Ag NPs formed predominantly spherical NPs and dispersed in a PMMA matrix with a uniform distribution. In the polymer matrix, the Ag-NPs are uniformly dispersed. It demonstrates a uniform dispersion of Ag and Graphene in PMMA composite with no discernible aggregation, indicating that ultrasonication is effective in the dispersion. Additionally, the surface of the hybrid nanocomposite appears both smooth and rough, attesting to its suitability, which will be further confirmed through electrical characterization. The micrographs show filler particles dispersed homogeneously within the polymer matrix. This dispersion state of the nanofiller (Gr, Ag) in the PMMA matrix is probably due to the reduction in the distance between the nanoparticles due to the increase of Gr-Ag concentration in the nanocomposites.

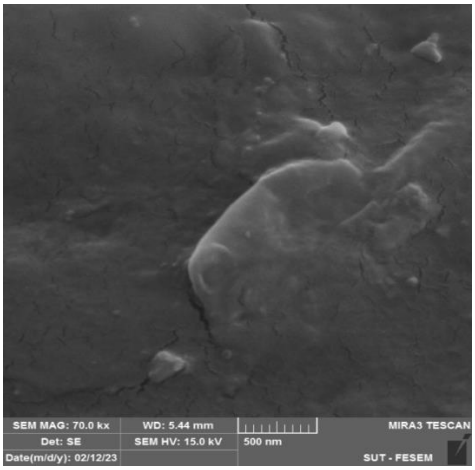

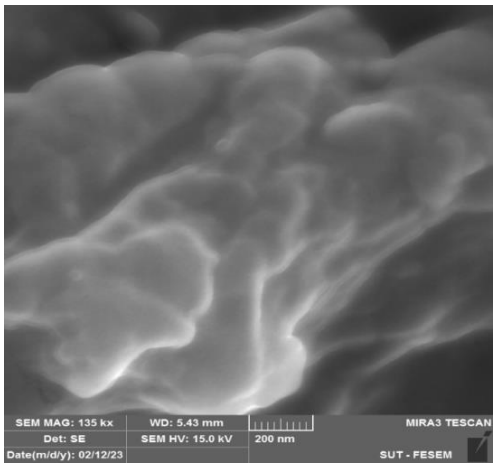

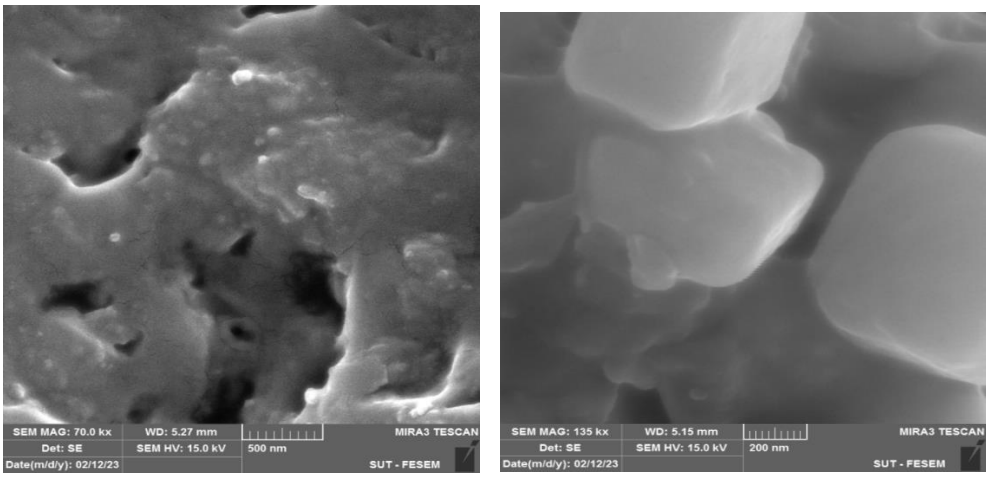

Figure 12. FE-SEM images of PMMA/Gr/Ag hybrid nanocomposites at (0.1%/0.5%) and (0.5%/0.5%)

4. Conclusions

The electrical conductivity related to hybrid composite demonstrates that D.C conductivity is around 1.6×10-6 S/cm, with a percolation critical concentration being reached at 0.5% for Ag and 0.5% for Graphene, as well as the fact that σac (ω) is frequency increases with increases in frequency. Concerning all PMMA/Gr/Ag hybrid composites, the frequency-dependent dielectric characteristics (ε′, ε′′, tan δ) reduce as the frequency region increases. It was discovered that Ag and graphene content have a significant impact on the SE of the provided composites. With 0.5wt%t of Graphene and Ag, the maximum EM attenuation of 11 dB at 12 GHz was attained. According to DTA, the exothermic type of reaction takes place between 200°C and 300°C, when weight loss is predominated. By uniform dispersion of silver and graphene particles within the PMMA matrix, which has a wide surface area because of the filler, PMMA/Gr/Ag hybrid composites exhibit superior interfacial bonding between the particles and matrix, according to FESEM results that appear a uniform integration as well as distribution of the filler particles by PMMA matrix with a homogenous deposition of prepared PMMA/Gr/Ag nanocomposites with concentrations of Ag, and graphene.

Acknowledgment

I would like to thank the staff of the Physics Department, Deanship of the College of Science, for their support in writing this research.

Conflict of Interest

The authors declare that they have no conflicts of interest.

Funding

None.

References

1. Faiza, S.; Munir, A.; Kashif, I. Polymeric textile-based electromagnetic interference shielding materials, their synthesis, mechanism and applications. *Journal of Industrial Textile* **2022,** *51(5)* ,7293–7358. https://doi:10.1002/app.44757.10.1002
2. Ahmed, N.; Abdulwahhabb, H.A.; Mustafa, A.A. Addition of Some Primary and Secondary Amines to Graphene Oxide and Studying Their Effect on Increasing its Electrical Properties. *Baghdad Science Journal* **2016,** *13(1),* 23-45. https://doi:10.1002/erp.43457.10.1342
3. Mustafa, A. H.; Ola, A. I.; Determine the Radon Gas Level Using the GIS Technique for Baghdad City" *Iraqi Journal of Science* **2018**, 59(1A), 218-226. https://doi:10.1002/ app .44757 .10.1002
4. Aya, H.M.; Asama, N.; Naje, R.; Ibrahim, K. Photoconductive Detector Based on Graphene Doping with Silver Nanoparticles. *Iraqi Journal of Science* **2022**, *63(12),* 5218-5231. https://doi:10.1002/rtp.43457.10.1442
5. Muthafar, F.; Jamil, A. Structural and dielectric properties of Zr doped BaTiO3synthesizedby microwave-assisted chemical route. *Iraqi Journal of Science* **2018,** *59(1),* 96-104. https://doi:10.1002/esd.43457.10.1376
6. Nadia, A.; Ali, A.; Abd-Elnaiem, S.; Hussein, A.; Khalil, H.; Alamri, R.; Hasan, S.A. Thermal and Mechanical Properties of Epoxy Resin Functionalized Copper and Graphene Hybrids using In-situ Polymerization Method. *Current Nanoscience* **2021,** *17(3), 23-35.*
7. Tabarak, M.A.; Seenaa, I.H. Improving the Mechanical Properties, Roughness, Thermal Stability, and Contact Angle of the Acrylic Polymer by Graphene and Carbon Fiber Doping for Waterproof Coatings. *Journal of Inorganic and Organometallic Polymers and Materials* **2022,** *32*, 3788–3796. https://doi:10.1002/ewe.43457.10.1345
8. Asmaa, N.; Mohammed, A.; Ali, N.A.; Hussein, S.I.; Alofi, A.S.; Abd-Elnaiem, A.M. Nano architectonics of Silver/Poly (Methyl Methacrylate) Films: Structure, Optical Characteristics, Antibacterial Activity, and Wettability. *Journal of Inorganic and Organometallic Polymers and Materials* **2023**, *33*, 694–706. https://doi:10.1002/ehy.43457.10.1399
9. Perna, R.; Modak, D.N.; Subhash, K. Electromagnetic Interference Shielding Effectiveness of Graphene-Based Conducting Polymer Nanocomposites. *Springer Proceedings in Physics* **2020,** *242(8),* 34-55. https://doi:10.1002/mkd.43457.10.1343
10. Bin, S.; Yang, Li.; Wentao, Z.; Wen-Ge, Z. Compressible Graphene-Coated Polymer Foams with Ultralow Density for Adjustable Electromagnetic Interference (EMI) Shielding. *J. ACS applied materials and interfaces* **2016**, *8*, 8050-8057. https://doi:10.1002/etr.43457.10.1321
11. Wei-Li, S.; Mao-Sheng, C.; Ming-Ming, L.; Song, B.; Chan-Yuan, W.; Jia, L.; Jie, Y.; Li-Zhen, F.; Flexible graphene/polymer composite films in sandwich structures for effective electromagnetic interference shielding. *J. Carbon*. **2014,** *66*, 67-76. https://doi:10.1002/ehy. 43457.10.1332
12. Limin, M.; Zhengang, L.; Jiubin, T.; Jian, L.; Xuemei, D.; Nicola, B.; Tianyi, L.; John, G.; Ling, H. Transparent Conducting Graphene Hybrid Films To Improve Electromagnetic Interference (EMI) Shielding Performance of Graphen**,** *J. ACS materials and interfaces* **2017,** *9(39),* 34221-34229. https://doi:10.1002/enh.43457.10.1355
13. Liam, A.; Premika, G.; Andrew, A.; Azadeh, M.; Nishar, H. Modelling, fabrication and characterization of graphene/polymer nanocomposites for electromagnetic interference shielding applications. *Journal Carbon Trends* **2021**, *4*, 12-34. https://doi:10.1002/evg.43457.10.1387
14. Aseel, A.K.; Hussein, K.R.; Electrical and thermal characteristics of MWCNTs modified carbon fiber/epoxy composite films. *Materials Science- Poland* **2019,** *37(4),* 34-44. https://doi:10.1002/esd.43457.10.1376

15. Al-Lamy, H.K.; Nasir, E.M.; Abdul-Ameer, H.J. Electrical properties of Cd_xse_{1-x} films at different thickness and annealing temperatures. *Digest Journal of Nanomaterials and Biostructures* **2020,** *15(1)*, 143–156. https://doi:10.1002/jud.43457.10.1390
16. Dash, K.; Hota, N.K.; Sahoo, B.P. Fabrication of thermoplastic polyurethane and polyaniline conductive blend with improved mechanical, thermal and excellent dielectric properties: Exploring the effect of ultralow-level loading of SWCNT and temperature. *J. Mater. Sci*. **2020,** *55*, 12568–12591. https://doi:10.1002/ety.43457.10.1322
17. Fan, P.; Wang, L.; Yang, J.; Chen, F.; Zhong, M. Graphene/poly (vinylidene fluoride) composites with high dielectric constant and low percolation threshold. *Nanotechnology* **2012,** *23*, 365702.
18. Farzaneh, F.; Pei, L.; Yap, R.; Udayashankar, K.;G. Gedler, M.; Antunes, J.I.; Velasco, R.O. Enhanced electromagnetic interference shielding effectiveness of polycarbonate/graphene nanocomposites foamed via 1-step supercritical carbon dioxide process. *Journal Materials and Design* **2016,** *90*, 906-914. https://doi:10.1002/enj.43457.10.1311
19. Habib, A.; Pierre, M.; Matias, R.; Hai, Z.; Mathematical Analysis of Plasmonic Nanoparticles: The Scalar Case. *Archive for Rational Mechanics and Analysis* **2017,** *224(2)*, 597–658.
20. Kadimi, A.; Benhamou, K.; Ounaies, Z.; Magnin, A.; Dufresne, A.; Kaddami, H.; Raihane, M. Electric Field Alignment of Nanofibrillated Cellulose (NFC) in Silicone Oil: Impact on Electrical Properties. *ACS Appl. Mater. Interfaces*, **2014,** *6*, 9418–9425. https://doi:10.1002/elo. 43457.10.1332
21. Kareem, A.A.; Rasheed, H.K.; Nasir, E.M.; Influence methods of preparation on the thermal stability of polyimide/silica dust. *Polymer Bulletinthis link is disabled* **2022,** *79(8)*, 6617–6626.
22. Liu, W.; Lee, S.W.; Lin, D.; Shi, F.; Wang, S.; Sendek, A.D.; Cui, Y.; Enhancing ionic conductivity in composite polymer electrolytes with well-aligned ceramic nanowires. *Nat. Energy*, **2017,** *2*, 17035. https://doi:10.1002/hyd.43457.10.1354
23. Quan, W.; Junbo, C.; Weifei, W.; Zhendong, H.; Xueqing, L.; Tianli, R.; Yuwei, C.; Jianming, Z. Contributing Factors of Dielectric Properties for Polymer Matrix Composites. *Polymers*, **2023,** *15(590)*. 23-45. https://doi:10.1002/bhg.43457.10.1344
24. Thakur, V.K.; Gupta, R.K. Recent Progress on Ferroelectric Polymer-Based Nanocomposites for High Energy Density Capacitors: Synthesis, Dielectric Properties, and Future Aspects. *Chem. Rev*. **2016,** *116*, 4260–4317. https://doi:10.1002/uyd.43457.10.1309
25. Xinyang, L.; Guilong, W.; Chunxia, Y.; Jinchuan, Z.; Aimin, Z. Mechanical and EMI shielding properties of solid and microcellular TPU/ nano graphite composite membranes. *Polymer Testing*, **2021,** *93*, 106891. https://doi:10.1002/hyg.43457.10.1765
26. Israa, M.R.; Yousif, I.M.; Takialdin, A.H. Interactions Investigation of New Composite Material Formed from Bauxite and Melamine-Urea Formaldehyde Copolymer. *Ibn Al-Haitham Journal. for Pure & Appl. Sci*. **2016**, *29*(*1*), 181–192. https://doi.edu.iq/index.php/j/article/view/57
27. Mingye, W.L.; Ma, B.L.; Wenjian, Z.; Hao, Z.; Guangshun, W.; Yudong, H.; Guojun, S. One-step generation of silica particles onto graphene oxide sheets for superior mechanical properties of epoxy composite and scale application. *Composites Communications* **2020**, *22*, 1–7. https://doi.10.science /article/abs/pii/S2452213920302424
28. Xiaomin, Y.; Bo, Z.; Xun, C.; Jianjun, L.; Kun, Q.; Junwei, Yu. Improved interfacial adhesion in carbon fiber/epoxy composites through a waterborne epoxy resin sizing agent. *Journal of Applied Polymer Science* **2017**, *134(17)*, 1–11, https://doi:10.1002/app.44757.10.1002
29. Adil, I.K.; Dhefaf, H.B.; Zainab, S.A. The Effect of Phoenix Dactylifera L. Pinnae Reinforcement on The Mechanical and Thermal Properties of Polymer Composite. *Journal of the college of basic education* **2019**, *104(25*), 339–349. https://doi:index.php/cbej/article /view/4654

30. Darbyshire, J.L. Mapping Sources of Noise in an Intensive Care Unit. *Anesthesia.* **2019,** *74(8),* 18–25. https://doi.org/10.15251/NHB.2023.543.908